Tools and Resources

Rapid Production of Pure Recombinant Actin Isoforms in *Pichia pastoris*

Tomoyuki Hatano*[1], Salvatore Alioto[2], Emanuele Roscioli[1], Saravanan Palani[1], Scott T. Clarke[1], Anton Kamnev[1], Juan Ramon Hernandez-Fernaud[3], Lavanya Sivashanmugam[1], Bernardo Chapa-Y-Lazo[1], Alexandra M. E. Jones[3], Robert C. Robinson[4, 5, 6], Karuna Sampath[1], Masanori Mishima[1], Andrew D. McAinsh[1], Bruce L. Goode[2] and Mohan K. Balasubramanian*[1]

[1]Centre for Mechanochemical Cell Biology and Division of Biomedical Sciences, Warwick Medical School, University of Warwick, Coventry CV4 7AL, UK. [2]Department of Biology, Brandeis University, Waltham, MA. [3]School of Life Sciences, University of Warwick, Coventry, UK CV4 7AL. [4]Institute of Molecular and Cell Biology, A*STAR (Agency for Science, Technology, and Research), Singapore 138673, Singapore. [5]Department of Biochemistry, National University of Singapore, Singapore 117597, Singapore. [6]Research Institute for Interdisciplinary Science, Okayama University, Okayama, 700-8530, Japan.

*Author for correspondence: Tomoyuki Hatano (T.Hatano@warwick.ac.uk) and Mohan Balasubramanian (m.k.balasubramanian@warwick.ac.uk)

JCS Advance Online Article. Posted on 13 March 2018

Abstract

Actins are major eukaryotic cytoskeletal proteins, which perform many important cell functions, including cell division, cell polarity, wound healing, and muscle contraction. Despite obvious drawbacks, muscle actin, which is easily purified, is used extensively presently for biochemical studies of actin cytoskeleton from other organisms / cell types. Here we report a rapid and cost-effective method to purify heterologous actins expressed in the yeast *Pichia pastoris*. Actin is expressed as a fusion with the actin-binding protein thymosin β4 and purified using an affinity tag introduced in the fusion. Following cleavage of thymosin β4 and the affinity tag, highly purified functional full-length actin is liberated. We purify actins from *S. cerevisiae*, *S. pombe*, and the β- and γ-isoforms of human actin. We also report a modification of the method that facilitates expression and purification of arginylated actin, a form of actin thought to regulate actin dendritic networks in mammalian cells. The methods we describe can be performed in all laboratories equipped for molecular biology, and should greatly facilitate biochemical and cell biological studies of the actin cytoskeleton.

Introduction

Actin is one of the most abundant eukaryotic proteins, which assembles into one of the main cytoskeletal polymers in eukaryotic cells. The actin cytoskeleton is vast, and cells express hundreds of proteins that associate with actin to control its polymerization, stability, spatial organization, and harness it to a wide spectrum of biological tasks, including muscle contraction, intracellular transport, cell motility, cell and tissue morphogenesis, cell adhesion, transcriptional regulation, and DNA damage (reviewed in Misu et al., 2017; Rottner et al., 2017; Skruber et al., 2018). As such, the study of actin has extended itself into almost all branches of biological research, creating a major need for biochemically characterizing the actin regulatory effects of numerous proteins from diverse model organisms, e.g., yeast, flies, worms, and mammals. To date, the majority of studies have used skeletal muscle actin (isolated from rabbits or chickens), because large quantities can be isolated at a reasonable cost-effectiveness. However, there are some major drawbacks to using muscle actin, including the heterogeneity in its post-translational modifications, and key differences in the properties of muscle actin from non-muscle actin isoforms and actin in different species (Bergeron et al., 2010; Kijima et al., 2016; Müller et al., 2013; Takaine and Mabuchi, 2007; Ti and Pollard, 2011; Wen et al., 2008; Wen and Rubenstein, 2005). These considerations have led to a need to develop new methods to purify actins, so that physiologically relevant biochemical and cell biological studies may be undertaken.

In this manuscript we describe a method to purify recombinant actin through expression in the yeast *Pichia pastoris*. We purify *S. cerevisiae*, *S. pombe*, and β- and γ- isoforms of human actin in a form that is functional *in vitro* and *in vivo*.

Results

To develop an easy and cost-effective method for purification of recombinant actins, we used the methylotrophic yeast *Pichia pastoris*, which is an excellent organism to express heterologous proteins (Gellissen, 2000; Macauley-Patrick et al., 2005). To reduce cross-contamination with endogenous *P. pastoris* actin, we introduced a strategy that blocks co-polymerization of recombinant actin with the host actin, both during cell growth and during purification. This was achieved by fusing the actin monomer binding protein thymosin β4 (Tβ4) sequence to the C-terminus of the actin coding sequence, with a short intervening in-frame linker [schematic in Figure 1A; (Noguchi et al., 2007)]. Fusion of actin to Tβ4 leads to intramolecular interactions preventing polymerization of the heterologous actin. A His tag (eight consecutive Histidine repeat, 8His) was further added to the C-terminus of the actin-Tβ4 fusion to facilitate affinity purification. Importantly, since the actin coding sequence ends with a highly conserved phenylalanine residue (cleavage site for chymotrypsin), and since all other phenylalanine residues are buried (Jacobson and Rosenbusch, 1976), incubation of the fusion protein with chymotrypsin releases native, untagged actin. This Tβ4-fusion purification approach has been used for heterologous actin expression in *Dictyostelium* and insect cells (Huang et al., 2016; Kijima et al., 2016; Noguchi et al., 2007; Xue et al., 2014). However, we reasoned that heterologous actin expression in *P. pastoris* would provide a much easier alternative, which could be used in virtually any laboratory equipped for molecular biology.

As a test case, we first expressed actin from *Saccharomyces cerevisiae* (UniProtKB entries: ACT_YEAST) where the actin cytoskeleton has been extensively characterized through genetics, biochemistry, and microscopy (Engqvist-Goldstein and Drubin, 2003; Moseley and Goode, 2006). Furthermore, since several biochemical studies in *S. cerevisiae* have used native actin purified from yeast cells, we reasoned that the vast existing knowledge of *S. cerevisiae* actin properties would help evaluate the functionality of the heterologously expressed *S. cerevisiae* actin. We were able to purify *S. cerevisiae* actin to near homogeneity after only a small number of steps, including binding to Ni-NTA resin, cleavage with chymotrypsin, and a cycle of polymerization and depolymerization (Figure 1B). The Ni-NTA bound fraction did not contain a prominent band at ~42 kDa, suggesting that native *P. pastoris* actin (UniProtKB entries: ACT_KOMPG) did not co-purify appreciably (Figure 1B). Next, we compared the polymerization properties of *S. cerevisiae* actin purified from *S. cerevisiae* (“Native”) versus *S. cerevisiae* actin purified from *P. pastoris* (“Recombinant”). We found that actin filament elongation rates were nearly identical, both in the presence and absence of a yeast formin (Bnr1) and yeast profilin (Pfy1) (Figure 1C and D). As expected, addition of Pfy1 alone, without the formin, marginally reduced the rate of elongation of native and recombinant Act1 polymers (Figure 1C and D), which we have also observed for profilins from several different species. We also found that there was no difference in average filament length over time for native and recombinant Act1 (Figure 1C and D). Based on these results, we conclude that recombinant Act1 has polymerization properties comparable to native Act1, and thus can be used reliably for biochemical studies.

To test the versatility of the heterologous actin expression system, we also attempted to express and purify fission yeast *Schizosaccharomyces pombe* actin (UniProtKB entries: ACT_SCHPO, "SpAct1"), since this organism has been used extensively in studies of the actin cytoskeleton and cytokinesis (Mishra et al., 2014; Pollard and Wu, 2010). We expressed and purified SpAct1 as actin-Tβ4-His fusion using the same steps used to purify *S. cerevisiae* actin (Figure 2A). Similar to *S. cerevisiae* Act1, the Ni-NTA bound fraction did not show major contamination with *P. pastoris* actin (Figure S1A; lane marked as uncleaved). N-terminal integrity was confirmed by immunoblotting using human γ-actin antibodies; *S. pombe* actin was recognized by antibodies against human γ-actin, consistent with the N-terminal sequence conservation between *S. pombe* and human γ-actin (Figure 2A). We note that SpAct1 was more prone to proteolysis compared to *S. cerevisiae* Act1 (Figure 2A), possibly reflecting some exposure of additional chymotrypsin sites.

We next asked whether we could express and purify the two human non-muscle actin isoforms, β- and γ-actin (UniProtKB entries: ACTB_HUMAN and ACTG_HUMAN, respectively). It is noteworthy that preparations of human non-muscle actins expressed in insect cells typically contain co-purifying host actin (Bergeron et al., 2010) and actin purified from human non-muscle cells or animal sources contains a mixture of β- and γ-isoforms. Similar to the yeast actins, the Ni-NTA bound fraction showed no major contamination with *P. pastoris* actin (Figure S1A; lane marked as uncleaved). Mass spectrometric analysis of β- and γ- actin detected all peptides derived from trypsin or chymotrypsin digestion of the expressed actins including N-terminal unique peptides. Mass spectrometry results are shown in supplemental table 1 and 2, and homogeneity of the purified actin is discussed in the legend to Figure S2 (see also Figure 4C). Immunoblotting of the purified actins with monoclonal antibodies against human β- and γ- actin supports N-terminal integrity of these proteins (Figure 2A).

To test the biochemical activities of purified SpAct1, and human β- and γ-actins, we performed sedimentation assays in the presence or absence of the actin polymerization inhibitor Latrunculin A (LatA) (Figure 2B). In low ionic strength buffer (G-buffer), like rabbit muscle actin, all recombinant actins remained in the supernatant fraction after ultracentrifugation. However, under polymerization conditions, after the addition of $MgCl_2$ and KCl, the muscle actin and recombinant actins shifted primarily to the pellet fractions indicating polymerization (Figure 2B). Furthermore, although solvent DMSO alone did not affect pelleting, incubation with Latrunculin-A blocked the polymerization of all actins. Further, *in vitro* polymerization assays, monitored by rhodamine-phalloidin staining, demonstrated that the recombinant *S. pombe* and human β- and γ-actins polymerized normally into filaments (Figure 2C).

To examine whether β- and γ-actins can be incorporated into cellular actin cytoskeletal networks, we labelled β- and γ-actins with Alexa Fluor 488 and Tetramethylrhodamine (TMR), respectively (schematic representation of the strategy is shown in Figure 3A and β-actin labelled with Alexa Fluor 488 is shown in Figure 3B), and injected into zebrafish embryos. We found that both actin isoforms could be efficently incorporated into the actin cytoskeleton at cell-cell contacts (Figure 3C). In addition, we injected β- and γ-actins labelled with Alexa Fluor 488 and TMR, respectively, into human RPE1 cells. The injected actins co-localized and assembled into native actin cytoskeleton-like structures and time-lapse imaging revealed their incorporation into dynamic filamentous structures

(Figure 3D and supplemental movie). From these results, we conclude that the labelled β- and γ-actins are active and readily decorate filamentous actin networks in RPE cells and zebrafish embryos.

Having established a simple method to purify large quantities of heterologous actins in *P. pastoris*, we next adapted this method to the production of arginylated actin, since human β-actin exists in both arginylated and non-arginylated forms (Karakozova et al., 2006). Arginylated actin appears to play key roles in actin filament assembly in the leading edge dendritic networks. To express and purify arginylated β-actin, we created a construct, which directs expression of a quadruple fusion containing *S. cerevisiae* ubiquitin-R-β-actin-Tβ4-His (Figure 4A). This fusion protein was expressed in *P. pastoris* and the ubiquitin moiety was cleaved by the endogenous ubiquitin-specific protease (Bachmair et al., 1986). R-β-actin-Tβ4-His was then purified as before and following cleavage with chymotrypsin, R-human β-actin (R-Actb) was isolated to near homogeneity (results of mass spectrometric analysis are shown in supplemental table 1 and 2 and the assessment of the homogeneity of the purified actin is discussed in the legend to Figure S2). An antibody against arginylated actin strongly recognized R-Actb, but only very weakly recognized unmodified Actb (Figure 4B). Mass spectrometric analysis detected the N-terminal arginylated peptide (Figure 4C and supplemental table 1). These results strongly indicated the N-terminal integrity of the R-Actb. Note that R-Actb runs slightly faster in SDS-PAGE probably reflecting different structural states of unmodified and arginylated β-actin in complex with SDS (Figure 4B and Figure S1B). The faster migration of R-Actb has also been reported by other investigators (Saha et al., 2010) We also found the R-Actb could be polymerized *in vitro*, suggesting that R-Actb purified from *P. pastoris* is functional (Figure 4D).

Discussion

In summary, we have developed a simple and rapid method, which requires only standard laboratory equipment, to purify large quantities of any specific actin isoform. The plasmids we describe will be deposited in Addgene. Investigators should be able to clone any actin gene of interest into these vectors, transform *P. pastoris,* and quickly purify the actin for biochemical characterization, and/or labelling and introduction into cells for live imaging.

We successfully purified human non-muscle β- and γ-actins, and actins from *S. cerevisiae* and *S. pombe*. Approximately 0.5-1 mg of actin is purified from a 1 L culture of cells grown in standard flasks (about 10 g of cells from 1 L saturated culture). Using the method we describe, actin from virtually any eukaryotic organism can be isolated and used to study the biochemical effects of actin binding proteins from the same species, improving the physiological relevance of the results. This method will also enable studies comparing the different actin isoforms, isolated to homogeneity, in the absence of other contaminating isoforms. Furthermore, we used this method to produce arginylated actin, which opens exciting avenues to characterizing actins with different post-translational modifications (Karakozova et al., 2006; Saha et al., 2010; Zhang et al., 2010). Finally, this method will enable purification to homogeneity of actins carrying point mutations that cause different human diseases (Laing et al., 2009; Nowak et al., 1999; Rivière et al., 2012), and use these purified mutants in biochemical drug screens. Thus, basic and translational studies will be positively impacted by the simple actin purification method we describe.

Actins undergo a variety of post-translational modifications and although some post-translational modifications occur in *Pichia pastoris*, other modifications do not. In future, it will be important to develop synthetic biology tools (such as expression of mammalian actin acetyl transferases and methyl transferases as well genetic code expansion for incorporation of modified amino acids) to express and purify actins carrying other modifications. Such tools will both facilitate elucidation of function of various actin modifications as well as promote physiologically relevant biochemical and cell biological experiments.

Methods

Plasmid used in this study

Actin coding sequences were cloned into pPICZc (invitrogen), which adds at the C-terminus an in-frame chymotrypsin cleavage site, linker sequence, thymosin β4, and His tag(Noguchi et al., 2007). These included *Homo sapiens* ACTB cDNA, synthesized *H. sapiens* ACTG1 cDNA (codon optimized for *Pichia pastoris*), the *Schizosaccharomyces pombe act1* gene, and the *Saccharomyces cerevisiae ACT1* gene (codon optimized for *P. pastoris*).

SDS-PAGE and immunoblotting

Samples were fractionated on 12% SDS-PAGE gels (Acrylamide:bis-acrylamide 37.5:1, #1610158, Bio-Rad), and stained with Coomassie Brilliant Blue (CBB) with InstantBlue (Expedeon). For immunoblotting, proteins were transferred to a nitrocellulose membranes using a semi-dry blotting system (Trans Blot Turbo, BIO-RAD). Membranes were incubated at room temperature for 1 h in blocking buffer (5% skimmed milk in TBS containing 0.5% Tween 20 and 0.02% NaN_3), then incubated in 0.001 v/v% anti-Actb (#MABT825, Merck Millipore) or Actg1 (#MABT824, Merck Millipore) antibodies in blocking buffer at 4˚C for 2 h. Membranes were washed 4 times with TBS containing 0.5% tween 20, then incubated with 0.003 v/v% Anti-mouse IgG conjugated with Horse Radish Peroxidase (HRP). For immunoblotting in Supplemental figure 2B, HRP-conjugated antibodies against human actin C-terminus (#sc-1616, Santa Cruz Biotechnology) was used to detect β-, γ- and argniylated β-actin. Proteins were detected with ECL Western Blotting Detecting Reagent (#RPN2106, GE Healthcare).

P. pastoris culture and transformation

Composition of MGY and MM growth media and basic techniques for *P. pastoris* X-33 are described in the Pichia Expression Kit Instruction Manual (Invitrogen). *P. pastoris* X-33 was transformed with pPICZc-ACTB, ACTG1 or *S. pombe act1* or *S. cerevisiae ACT1*. Plasmid DNA was linearized with PmeI and transformed using the Lithium Chloride method. Transformants were selected on Yeast Extract Peptone Dextrose (YPD) plates containing 100 mg/L Zeocin (Gibco, #R25001) grown at 30˚C.

Purification of recombinant actins from *P. pastoris*

P. pastoris transformants were revived on YPD solid media. Cells were inoculated into 200 ml minimal glycerol (MGY) liquid media composed of 1.34% yeast nitrogen base without amino acids (SIGMA Y0626), 0.00004% biotin and 1% glycerol and cultured at 30˚C, shaking at 220 rpm. Culture media was diluted 1.5 L by addition of 1.3 L fresh MGY media, and cells were cultured at 30˚C, 220 rpm until OD600 = 1.5. Cells were pelleted by centrifugation at 7000 rpm at 25˚C for 10 min (Thermo Fisher Scientific #F9-

6 x 1000 LEX rotor). Cells were washed once with sterilized water and re-suspended into 2 L minimal methanol (MM) media, composed of 1.34% yeast nitrogen base without amino acids (Sigma Y0626), 0.00004% biotin and 0.5% methanol. Cells were cultured in four separate 2 L flasks (500 mL culture each) at 30˚C, 220 rpm for 1.5-2 days. 0.5 % methanol was added every 24 h of culturing. Cells were pelleted as above, yielding about 10 g wet weight of cells per 1 L culture. Cells were washed once with water and resuspended in 30 mL H_2O. The suspension was dripped into liquid nitrogen to form frozen beads, which were stored at -80˚C until use.

For each preparation, 30 g of frozen cells was used, which was loaded into 8 grinder tubes (#6751, SPEX® SamplePrep) pre-cooled with liquid nitrogen and ground in a Freezer mill (#6870, SPEX® SamplePrep) in a liquid nitrogen bath. Duration of the grinding was 1 min with 14 cycles / second. The grinding was repeated 30 times at 1 min intervals. Liquid nitrogen was re-filled every 10 cycles of grinding. The lysate powder was resolved in an equal amount of 2 x Binding buffer composed of 20 mM imidazole (pH 7.4), 20 mM HEPES (pH 7.4), 600 mM NaCl, 4 mM $MgCl_2$, 2 mM ATP (pH 7), 2x concentration of protease inhibitor cocktail (cOmplete, EDTA free #05056489001, Roche), 1 mM phenylmethylsulfonyl fluoride (PMSF) and 7 mM β-mercaptoethanol (β-ME). The lysate was sonicated on ice (10 sec with 60% amplitude, Qsonica Sonicators) until all aggregates were resolved. The lysate was centrifuged at 4˚C at 4000 rpm for 15 min (Eppendorf #A-4-81 rotor) to remove intact cells and debris, then further cleared by centrifugation at 4˚C at 15000 rpm for 1 h (Thermo Fisher Scientific #A23-6 x 100 rotor). The supernatant was passed through a 0.22 µm filter (Corning #431097) and incubated with 1 ml Nickel resin (Thermo Scientific #88222) at 4˚C for 1-1.5 h. The resin was pelleted down by centrifugation at 4˚C at 2500 rpm for 5 min (Eppendorf #A-4-81 rotor) and washed with 25 mL ice-cold binding buffer composed of 10 mM imidazole (pH 7.4), 10 mM HEPES (pH 7.4), 300 mM NaCl, 2 mM $MgCl_2$, 1 mM ATP (pH 7), protease inhibitor cocktail (complete, EDTA free #05056489001, Roche), 1 mM PMSF and 7 mM β-ME. The resin was loaded into an open column (BioRad, #731-1550) and washed first with ice-cold 20 mL Binding buffer, then with 45 mL ice-cold G-buffer composed of 5 mM HEPES (pH 7.4), 0.2 mM $CaCl_2$, 0.01 w/v% NaN_3, 0.2 mM ATP (pH 7) and 0.5 mM dithiothreitol (DTT). The resin was resuspended in 6 mL ice-cold G-buffer containing 5 µg/ml TLCK treated chymotrypsin (Sigma #C3142-10MG) and incubated overnight at 4˚C. The chymotrypsin was inactivated by addition of PMSF to 1 mM and incubated for 30 min on ice. The eluate was then collected into a tube. Actin retained on the resin was eluted with 12 mL G-buffer and all the elution fractions were combined. The eluate was concentrated using a 30 kDa cut-off membrane (Sigma-Aldrich #Z677892-24EA) and the final volume adjusted to 900 µl with ice-cold G-buffer. Actin was polymerized by addition of 100 µl 10x MEK buffer, composed of 20 mM $MgCl_2$, 50 mM glycol-bis(2-aminoethylether)-N,N,N′,N′-tetraacetic (EGTA) and 1 M KCl for 1 h at room temperature. F-actin was pelleted by ultracentrifugation for 1 h at room temperature at 45000 rpm (Beckman TLA-55 rotor) and re-suspended in 1 mL ice cold G-buffer. F-actin was depolymerized by dialysis against 1 L G-buffer at 4˚C for 2 days. Dialysis buffer was exchanged every 12 h. Any remaining F-actin was pelleted by ultracentrifugation at room temperature at 45000 rpm for 30 min (Beckman TLA-55 rotor) and actin in the supernatant was concentrated to 100 µM using a 30 kDa cut-off membrane (Sigma-Aldrich #Z677892-24EA). The concentration of actin was determined by absorbance at 290 nm (ε290 = 0.63 (/mg/ml/cm)) using a NanoDrop 2000c spectrophotometer (Thermo Fisher Scientific).

Purification of native yeast Act1 and recombinant Pfy1 (Profilin) and Bnr1

Act1 was isolated from *S. cerevisiae* as described(Cook et al., 1992), except using G-buffer consisting of 5 mM HEPES, pH 7.6, 0.2 mM $CaCl_2$, 0.2 mM ATP, 2 mM β-mercaptoethanol. Rabbit muscle actin was purified from acetone powder following a protocol from Pardee & Spudich(Pardee and Spudich, 1982). Rabbit muscle actin was labeled with Oregon Green (OG), and the concentration and labeling efficiency were determined as described(Kuhn and Pollard, 2005). 6His-tagged Bnr1 (FH1-FH2-C) was overexpressed in *S. cerevisiae* and purified by nickel chromatography and gel filtration as described(Moseley et al., 2006). Untagged *S. cerevisiae* profilin (Pfy1) was expressed and purified from *E. coli* by anion-exchange chromatography and gel filtration as described(Moseley et al., 2004).

Total internal reflection fluorescence (TIRF) microscopy

Glass coverslips (24 × 60 mm #1.5; Fisher Scientific, Pittsburg, PA) were sonicated for 1 h in 2% Micro-90 detergent, followed by 1 h sonication in 100% ethanol, then 30 min sonication in 0.1 M KOH and ddH20, respectively. Cleaned coverglass was stored in 100% ethanol prior to use. Before each experiment, coverslips were rinsed with ddH20, dried with N_2, and coated by applying 120 µL of 2 mg/mL methoxy-poly(ethylene glycol) (mPEG)- silane MW 2,000 (Laysan Bio, Arab, AL) and 4 µg/mL biotin-PEG-silane MW 3,400 (Laysan Bio, Arab, AL) resuspended in 80% ethanol, pH 2.0. Coated coverslips were incubated for 16 h at 70ºC. Flow cells were assembled by rinsing PEG-coated coverslips with ddH20, drying with N_2, and adhering to µ-Slide VI0.1 (0.1 mm × 17 mm × 1 mm) flow chambers (Ibidi, Martinsried, Germany) with double-sided tape (2.5 cm × 2 mm × 120 µm) sealed with five-minute epoxy resin (Devcon, Riviera Beach, FL). Flow cells were incubated for 1 min with 1% BSA, then incubated for 1 min with TIRF buffer (10 mM imidazole pH 7.4, 50 mM KCl, 1 mM $MgCl_2$, 1 mM EGTA, 0.2 mM ATP, 10 mM DTT, 15 mM glucose, and 0.25% methyl cellulose [4000 cP]). TIRF reactions were initiated by adding 1 µM actin (20% OG-labeled) to premixed actin-binding proteins. Reactions were introduced into the flow chamber, which was then mounted on the microscope stage for imaging. Time between addition of actin and the start of TIRF recording was 180 s. Time lapse imaging was performed on a Nikon-Ti200 inverted microscope (Nikon Instruments) equipped with a 488 nm argon laser (150 mW; Melles Griot, Carlsbad, CA), a 60× Apo oil-immersion TIRF objective (NA 1.49; Nikon Instruments), and an EMCCD camera with a pixel size of 0.267 µm (Andor), and running NIS-Elements (Nikon Instruments). Focus was maintained by the Perfect Focus system (Nikon Instruments). Images were collected at 5 s intervals for 15 min. Background fluorescence was removed from each image in a stack using the background subtraction tool (rolling ball radius, 50 pixels) in ImageJ. Minimal contrast enhancement or changes to the black level were applied to entire stack to improve image quality for analysis and display. Filament elongation rates were determined from n ≥ 10 filaments in each of three independent experiments. Filament length was measured using the freehand line tool in ImageJ. Elongation rates were determined by plotting filament length versus time, where the rate is the slope. To express rates in actin subunits s^{-1}, we used the conversion factor of 374 subunits per micron of F-actin.

Cysteine labelling with fluorophore-maleimide

For experiments in which we introduced Alexa-488-actin or TMR-actin into cells, we directly labeled Cys^{374}, the C-terminal residue of actin. Actin released by chymotrypsin digestion and eluted form the Nickel resin (see purification details above) was concentrated to ~1.3 mg/ml, and then polymerized for 1 h at 4˚C by addition of 2 mM $MgCl_2$ and 100 mM KCl. Alexa Fluor 488-C5-maleimide (Thermo Fisher Scientific #A10254) or Tetramethylrhodamine (TMR)-5-maleimide (Thermo Fisher Scientific #T6027) dissolved in dimethyl sulfoxide as a 3 mM stock was added drop-wise to reach a 3.5 molar excess of dye to actin, and incubated for 1 h at room temperature in the dark. The reaction was quenched by addition of 10 mM DTT, and the reaction was cleared of any precipitated dye by centrifugation at 4˚C at 5000 rpm for 10 min (Eppendorf FA-45-24-11). F-actin was pelleted by ultracentrifugation at room temperature at 45000 rpm for 1 h (Beckman TLA-55 rotor). The pellet was re-suspended and dialyzed against G-buffer to depolymerize actin, as described above, and free fluorophore-maleimide was separated from labelled actin using Sephadex G-25 (PD MidiTrap G-25, GE Healthcare #28-9180-07). The concentration of fluorophore-labelled actin was measured by absorbance at 290 (actin), 495 (Alexa Fluor 488), and 550 nm (TMR) on a NanoDrop 2000c spectrophotometer (Thermo Fisher Scientific), and calculated using the following formula; Actin concentration (M)= A290 / (0.63 x 42000). The extinction coefficient of Alexa Fluor 488 at 495 nm is ε495=72,000 M−1 cm−1, with a correction factor for Alexa Fluor 488 absorbance at 290 nm of 0.138. Labelling efficiency was calculated as follows; (A495 / 72,000) / actin concentration (M). Purified actin was kept on ice in dark.

Mass spectrometry (MS) methods and analysis

50 µg of each purified protein were separated on 12% SDS-PAGE gel and stained with Coomassie G-250 (SimplyBlue SafeStain, Invitrogen). The actin gel band (~42KDa) was cut and in gel digested with trypsin and peptides concentrated and desalted on StageTips (1) Reversed phase chromatography with two columns, an Acclaim PepMap µ-precolumn cartridge 300 µm i.d. x 5 mm, 5 µm, 100 Å and an Acclaim PepMap RSLC 75 µm i.d. x 50 cm, 2 µm, 100 Å (Thermo Scientific) was used to separate tryptic peptides prior to mass spectrometric analysis. The columns were installed on an Ultimate 3000 RSLCnano system (Dionex) at 40C. Mobile phase buffer A was composed of 0.1% formic acid and mobile phase B was composed of acetonitrile containing 0.1% formic acid. Samples were loaded onto the µ-precolumn equilibrated in 2% aqueous acetonitrile containing 0.1% trifluoroacetic acid for 5 min at 10 µL min^{-1}, after which peptides were eluted onto the analytical column at 250 nL min^{-1} by increasing the mobile phase B concentration from 6% B to 25% over 31 min and to 37% for 10 min, followed by a 3 min wash at 80% B and a 10 min re-equilibration at 4% B. Eluting peptides were converted to gas-phase ions by means of electrospray ionization and analysed on a Thermo Orbitrap Fusion (Thermo Scientific). Survey scans of peptide precursors from 375 to 1500 m/z were performed at 120K resolution (at 200 m/z) with a 2x105 ion count target. The maximum injection time was set to 150 ms. Tandem MS was performed by isolation at 1.2 Th using the quadrupole, HCD fragmentation with normalized collision energy of 33, and rapid scan MS analysis in the ion trap. The MS2 ion count target was set to 5x103. The maximum injection time was 200 ms. Precursors with charge state 2–6 were selected and sampled for MS2. The dynamic exclusion duration was set to 40 s with a 10 ppm tolerance around the selected precursor and its isotopes. Monoisotopic precursor selection was turned on. The instrument was run in top speed mode. The acquired tandem mass spectrometry (MS/MS) mass spectra were

processed with SequestHT implemented on the Proteome Discoverer software version 2.2.0.388 for peptide and protein identifications against Homo sapiens proteome (UP000005640, containing 71,544 proteins) and Komagataella phaffii proteome (UP000000314, containing 5,073 proteins). The SequestHT node included the following parameters: Precursor Mass Tolerance 10 ppm, Fragment Mass Tolerance 0.6 Da, Dynamic Modifications were Oxidation of M (+15.995 Da), Acetyl of K (+42.011 Da), Methyl of K (+14.016 Da), Phospho of STY (+79.966 Da) and Acetyl protein N-term (+42.011 Da). The Static Modification was Carbamidomethyl of C (+57.021 Da). The level of confidence for peptide identifications was estimated with the Percolator node with decoy database search. FDR was set at 0.01 based on q-value.

F-actin sedimentation assays and imaging

Actin (12.5 µM) in G-buffer was mixed with 2 mM $MgCl_2$, 5 mM EGTA and 100 mM KCl for 1 h at 24˚C. To make a 0.5 mM Latrunculin A (LatA) solution, 10 mM LatA in dimethyl sulfoxide (DMSO) was first diluted to 2 mM with G-buffer, then further diluted to 0.5 mM in the reaction mixture (final concentration of DMSO 4%). The reaction mixture was ultracentrifuged in an Airfuge (Beckman Coulter) at 25 psi, room temperature for 30 min. Pellet and supernatant fractions were analysed on Coomassie-stained gels. For imaging actin filaments, actin (8.33 µM) in G-buffer was polymerized by addition of 2 mM $MgCl_2$, 5 mM EGTA, 100 mM KCl and 2% polyethylene glycol 20,000 (#8.17018.1000, Merck Millipore) and incubation at 24˚C for 1 h. 5% (v/v) rhodamine phalloidin (#R415, Thermo Fisher Scientific) or phalloidin-CF633 (#00046, Biotium) was added, and F-actin was imaged using an Andor Revolution XD spinning disk confocal system on a Nikon Eclipse Ti inverted microscope, Nikon Plan Apo Lambda 100×/1.45NA oil immersion objective lens, a spinning-disk system (CSU-X1; Yokogawa), and an Andor iXon Ultra EMCCD camera. Images were acquired at the pixel size of 80 nm/pixel using the Andor IQ3 software. Laser lines at a wavelength of 561 or 640 nm was used for excitation.

Actin injection into Zebrafish embryos

Half mg/ml β- and γ-actin labelled with TMR were diluted tenfold in low ionic strength buffer (final composition: 5 mM HEPES (pH 7.4), 0.05 mM $CaCl_2$, 0.0025 w/v% NaN_3, 0.2 mM ATP and 0.5 mM DTT) and cleared polymerized actin by ultracentrifugation with Airfuge (BECKMAN COULTER) at 25 psi for 10 minutes at 4˚C.

Wild type embryos were obtained by natural mating using standard procedures in accordance with institutional animal care regulations at the University of Warwick. Approx. 0.113 nl of β- and γ-actin with TMR was injected into the blastoderm at the one cell stage. Embryos were thence dechorionated, embedded in 1 % low melting agarose on No. 0 coverslips (MatTek 35 mm uncoated dishes), and imaged at the animal pole; while maintained in egg water at 26°C. Images were acquired using Andor Revolution XD confocal systems, assembled on a Nikon Eclipse Ti inverted microscope, a spinning disc confocal Yokogawa CSU-X1 unit and an Andor iXon Ultra EMCCD camera. The β-actin injected embryos were imaged using a Nikon Plan Apo Lambda 20×/0.75NA objective lens; with a final pixel size of 0.35 µm/pixel using Andor IQ3 software. The γ-actin injected embryos were imaged using a Nikon Plan Apo Lambda 10×/0.45NA objective lens; with a final pixel size of 0.8 µm/pixel using Andor IQ3 software. A 561 nm laser lines was used for excitation. All images were acquired with a Z-step size of 0.5 mm. The image stacks were projected along the Z-axis (maximum intensity) using Fiji (Schindelin et al., 2012).

Cell culture

Immortalized (hTERT) diploid human retinal pigment epithelial (RPE1) cells were grown in DMEM/F-12 medium containing 10% fetal bovine serum (FBS), 2mM L-Glutamine, 100 U/ml penicillin and 100 µg/ml streptomycin. In each experiment, cells were plated 24 or 48 hours before imaging into a glass bottom FluoriDish (FD35-100, World Precision Instrument, Inc.).

Actin injection into human RPE1 cells and imaging

0.25 or 0.5 mg/ml β-actin labelled with Alexa Flour 488 and γ-actin with TMR were mixed in low ionic strength buffer composed of 5 mM HEPES (pH 7.4), 0.05 mM CaCl2, 0.0025 w/v% NaN3, 0.2 mM ATP and 0.5 mM DTT and cleared polymerized actin by ultracentrifugation with Airfuge (BECKMAN COULTER) at 25 psi for 10 minutes at 4˚C.

Microinjection was performed on an Olympus IX71 microscope, equipped with a 40x / 0.6 NA long distance objective and the Integra TI micromanipulator (Research Instruments Ltd), using the FemtoJet 4i microinjector (Eppendorf). G-actins were microinjected at room temperature into the cytoplasm of RPE1 cells using pre-pulled Femtotips II needles (Eppendorf). Tipically, in each experiment, cells from about 10 different fields were injected. To visualise the DNA, RPE1 cells were incubated, 1 hour before the injection, with DMEM/F-12 media containing 0.5µM of SiR-DNA far-red probe (Spirochrome). Dynamic live movies and static live images were acquired after the microinjection was completed.

Live-cell imaging was performed on an Olympus DeltaVision Elite microscope (Applied Precision, LLC) equipped with a Photometrics CoolSNAP HQ camera (Roper Scientific) and a stage-top incubator (TokaiHit) to maintain cells at 37ºC and 5% CO2. Temperature was further stabilized using a microscope enclosure (Weather station; Precision Control) held at 37ºC. Image stacks (10 x 0.5 µm optical sections) were acquired using the softWoRX 5.5 software every 10 minutes for a 5 hours period using a 40x / 1.3 NA oil-immersion objective. In each experiment, about 10 individual fields (1024 x1024 pixels) were imaged using the point visit function in softWoRX 5.5. Original movies were then deconvolved with the softWoRX 5.5 software and processed with Fiji (Schindelin et al., 2012).

Static live images were acquired using a confocal spinning-disk microscope (VOX UltraView; PerkinElmer, UK) equipped with a 100X / 1.4 NA oil-immersion objective and a Hamamatsu ORCA-R2 camera, controlled by Volocity 6.0 (PerkinElmer) running on a Windows 7 64-bit (Microsoft, Redmond, WA) PC (IBM, New Castle, NY). Temperature on the spinning disc was stabilized using a microscope enclosure (Solent Scientific) held at 37ºC. Image stacks were acquired over 50 z-slices separated by 0.2µm for a single timepoint using the 488, 561 and 640 nm wavelength lasers. Spinning disc images were exported from Volocity 6.0 in OME.TIFF format (The Open Microscopy Environment, UK). They were deconvolved in the 488 and 561 nm wavelengths within Huygens 4.1 (SVI), using point spread functions calculated from 100 nm TetraSpeck fluorescent microspheres (Invitrogen) using the Huygens 4.1 PSF distiller. Images were deconvolved in the 640 nm wavelength within Huygens 4.1 using a theoretical PSF. Deconvolved images were exported from Huygens 4.1 in r3d format (Applied Precision, Slovakia) and processed with Fiji (Schindelin et al., 2012).

Acknowledgements

We are grateful to members of the Balasubramanian laboratory for discussion. We thank Dr. Giacomo De Piccoli and Prof. Robert Cross for sharing equipment.

Competing interests

The authors declare no competing or financial interests.

Author Contributions

TH established the actin purification method and performed the most of experiments. SA and BLG performed TIRF microscopy experiments and analysed the data. TH, ER, ADM performed actin injection into human cells, acquired data, and interpretation of data. TH, STC and KS performed actin injection into zebrafish, acquired data, and interpretation of data. SP, JRHF and AMEJ performed mass spectrometric analysis of purified actins. AK acquired microscope images of actin filaments. LS help TH to purify recombinant actins. BCL provided rabbit muscle actin and RCR generated human β–actin plasmid and provided the original idea. TH and MKB, conceived the project, designed the experiments, and supervised the project. MM analysed data and provided critical advice for many experiments. TH, MKB and BLG wrote the manuscript. All authors reviewed the manuscript.

Funding

This work was supported by Wellcome Trust Senior Investigator Award (WT101885MA), a Wellcome Collaborative Award in Science (203276/Z/16/Z), a Royal Society Wolfson merit award (WM130042) and an European Research Council Advanced Grant (ERC-2014-ADG N° 671083) to MKB. BLG was supported by a grant from National Institute of Health (GM063691). ADM was supported by a Wellcome Trust Senior Investigator Award (grant 106151/Z/14/Z) and a Royal Society Wolfson Research Merit Award (grant WM150020). KS was funded by the Biotechnology and Biological Sciences Research Council (BB/L007525/1), Wellcome Warwick ISSF Quantitative Biomedicine Programme and Warwick Research Development Fund awards. RCR was supported by core funding from Institute of Molecular and Cell Biology (IMCB)/Agency for Science, Technology and Research (A*STAR). AMEJ thanks Proteomics Research Technology Platform for the contribution to the mass spectrometry analysis. STC was funded by a studentship from the Engineering and Physical Sciences Research Council.

References

Bachmair, A., Finley, D. and Varshavsky, A. (1986). In vivo half-life of a protein is a function of its amino-terminal residue. *Science* **234**, 179-86.

Bergeron, S. E., Zhu, M., Thiem, S. M., Friderici, K. H. and Rubenstein, P. A. (2010). Ion-dependent polymerization differences between mammalian beta- and gamma-nonmuscle actin isoforms. *J Biol Chem* **285**, 16087-95.

Cook, R. K., Blake, W. T. and Rubenstein, P. A. (1992). Removal of the amino-terminal acidic residues of yeast actin. Studies in vitro and in vivo. *J Biol Chem* **267**, 9430-6.

Engqvist-Goldstein, A. E. and Drubin, D. G. (2003). Actin assembly and endocytosis: from yeast to mammals. *Annu Rev Cell Dev Biol* **19**, 287-332.

Gellissen, G. (2000). Heterologous protein production in methylotrophic yeasts. *Appl Microbiol Biotechnol* **54**, 741-50.

Huang, S., Umemoto, R., Tamura, Y., Kofuku, Y., Uyeda, T. Q., Nishida, N. and Shimada, I. (2016). Utilization of paramagnetic relaxation enhancements for structural analysis of actin-binding proteins in complex with actin. *Sci Rep* **6**, 33690.

Jacobson, G. R. and Rosenbusch, J. P. (1976). ATP binding to a protease-resistant core of actin. *Proc Natl Acad Sci U S A* **73**, 2742-6.

Karakozova, M., Kozak, M., Wong, C. C., Bailey, A. O., Yates, J. R., Mogilner, A., Zebroski, H. and Kashina, A. (2006). Arginylation of beta-actin regulates actin cytoskeleton and cell motility. *Science* **313**, 192-6.

Kijima, S. T., Hirose, K., Kong, S. G., Wada, M. and Uyeda, T. Q. (2016). Distinct Biochemical Properties of Arabidopsis thaliana Actin Isoforms. *Plant Cell Physiol* **57**, 46-56.

Kuhn, J. R. and Pollard, T. D. (2005). Real-time measurements of actin filament polymerization by total internal reflection fluorescence microscopy. *Biophys J* **88**, 1387-402.

Laing, N. G., Dye, D. E., Wallgren-Pettersson, C., Richard, G., Monnier, N., Lillis, S., Winder, T. L., Lochmüller, H., Graziano, C., Mitrani-Rosenbaum, S. et al. (2009). Mutations and polymorphisms of the skeletal muscle alpha-actin gene (ACTA1). *Hum Mutat* **30**, 1267-77.

Macauley-Patrick, S., Fazenda, M. L., McNeil, B. and Harvey, L. M. (2005). Heterologous protein production using the Pichia pastoris expression system. *Yeast* **22**, 249-70.

Mishra, M., Huang, J. and Balasubramanian, M. K. (2014). The yeast actin cytoskeleton. *FEMS Microbiol Rev* **38**, 213-27.

Misu, S., Takebayashi, M. and Miyamoto, K. (2017). Nuclear Actin in Development and Transcriptional Reprogramming. *Front Genet* **8**, 27.

Moseley, J. B. and Goode, B. L. (2006). The yeast actin cytoskeleton: from cellular function to biochemical mechanism. *Microbiol Mol Biol Rev* **70**, 605-45.

Moseley, J. B., Maiti, S. and Goode, B. L. (2006). Formin proteins: purification and measurement of effects on actin assembly. *Methods Enzymol* **406**, 215-34.

Moseley, J. B., Sagot, I., Manning, A. L., Xu, Y., Eck, M. J., Pellman, D. and Goode, B. L. (2004). A conserved mechanism for Bni1- and mDia1-induced actin assembly and dual regulation of Bni1 by Bud6 and profilin. *Mol Biol Cell* **15**, 896-907.

Müller, M., Diensthuber, R. P., Chizhov, I., Claus, P., Heissler, S. M., Preller, M., Taft, M. H. and Manstein, D. J. (2013). Distinct functional interactions between actin isoforms and nonsarcomeric myosins. *PLoS One* **8**, e70636.

Noguchi, T. Q., Kanzaki, N., Ueno, H., Hirose, K. and Uyeda, T. Q. (2007). A novel system for expressing toxic actin mutants in Dictyostelium and purification and characterization of a dominant lethal yeast actin mutant. *J Biol Chem* **282**, 27721-7.

Nowak, K. J., Wattanasirichaigoon, D., Goebel, H. H., Wilce, M., Pelin, K., Donner, K., Jacob, R. L., Hübner, C., Oexle, K., Anderson, J. R. et al. (1999). Mutations in the skeletal muscle alpha-actin gene in patients with actin myopathy and nemaline myopathy. *Nat Genet* **23**, 208-12.

Pardee, J. D. and Spudich, J. A. (1982). Purification of muscle actin. *Methods Enzymol* **85 Pt B**, 164-81.

Pollard, T. D. and Wu, J. Q. (2010). Understanding cytokinesis: lessons from fission yeast. *Nat Rev Mol Cell Biol* **11**, 149-55.

Rivière, J. B., van Bon, B. W., Hoischen, A., Kholmanskikh, S. S., O'Roak, B. J., Gilissen, C., Gijsen, S., Sullivan, C. T., Christian, S. L., Abdul-Rahman, O. A. et al. (2012). De novo mutations in the actin genes ACTB and ACTG1 cause Baraitser-Winter syndrome. *Nat Genet* **44**, 440-4, S1-2.

Rottner, K., Faix, J., Bogdan, S., Linder, S. and Kerkhoff, E. (2017). Actin assembly mechanisms at a glance. *J Cell Sci* **130**, 3427-3435.

Saha, S., Mundia, M. M., Zhang, F., Demers, R. W., Korobova, F., Svitkina, T., Perieteanu, A. A., Dawson, J. F. and Kashina, A. (2010). Arginylation regulates intracellular actin polymer level by modulating actin properties and binding of capping and severing proteins. *Mol Biol Cell* **21**, 1350-61.

Schindelin, J., Arganda-Carreras, I., Frise, E., Kaynig, V., Longair, M., Pietzsch, T., Preibisch, S., Rueden, C., Saalfeld, S., Schmid, B. et al. (2012). Fiji: an open-source platform for biological-image analysis. *Nat Methods* **9**, 676-82.

Skruber, K., Read, T. A. and Vitriol, E. A. (2018). Reconsidering an active role for G-actin in cytoskeletal regulation. *J Cell Sci* **131**.

Takaine, M. and Mabuchi, I. (2007). Properties of actin from the fission yeast Schizosaccharomyces pombe and interaction with fission yeast profilin. *J Biol Chem* **282**, 21683-94.

Ti, S. C. and Pollard, T. D. (2011). Purification of actin from fission yeast Schizosaccharomyces pombe and characterization of functional differences from muscle actin. *J Biol Chem* **286**, 5784-92.

Wen, K. K., McKane, M., Houtman, J. C. and Rubenstein, P. A. (2008). Control of the ability of profilin to bind and facilitate nucleotide exchange from G-actin. *J Biol Chem* **283**, 9444-53.

Wen, K. K. and Rubenstein, P. A. (2005). Acceleration of yeast actin polymerization by yeast Arp2/3 complex does not require an Arp2/3-activating protein. *J Biol Chem* **280**, 24168-74.

Xue, B., Leyrat, C., Grimes, J. M. and Robinson, R. C. (2014). Structural basis of thymosin-β4/profilin exchange leading to actin filament polymerization. *Proc Natl Acad Sci U S A* **111**, E4596-605.

Zhang, F., Saha, S., Shabalina, S. A. and Kashina, A. (2010). Differential arginylation of actin isoforms is regulated by coding sequence-dependent degradation. *Science* **329**, 1534-7.

Figures

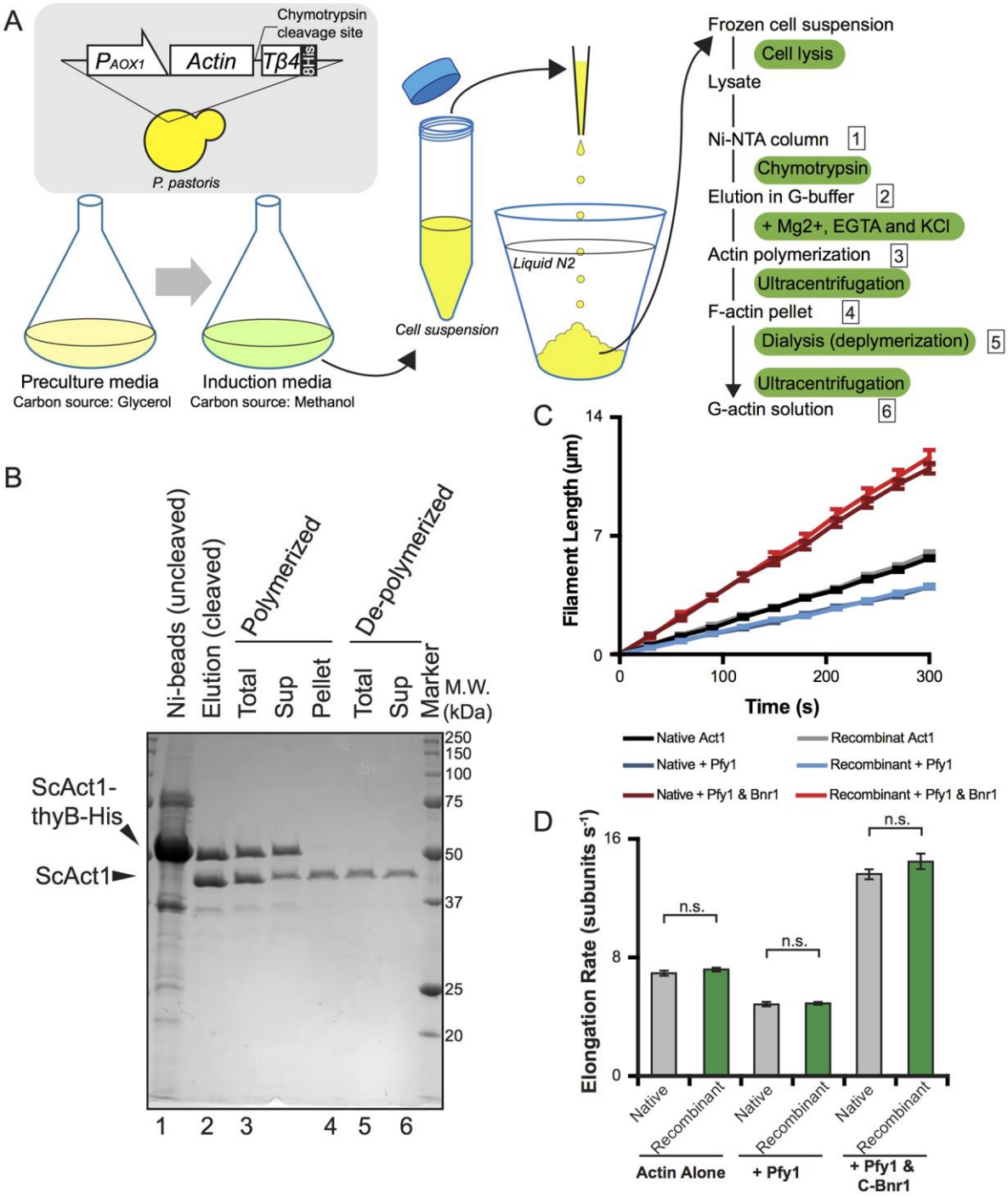

Figure 1. Purification of assembly-competent recombinant *Saccharomyces cerevisiae* Act1 from *Pichia pastoris*
(A) Flow chart of actin purification method (for details see Materials and Methods). **(B)** Coomassie-stained gel (CBB) showing purified recombinant *Saccharomyces cerevisiae* Act1. Numbering (1-6) at the bottom corresponds to numbers in flow chart in (A). **(C)** TIRF microscopic analysis of actin filament growth, comparing Act1 purified from *S. cerevisiae* ("Native") and recombinant Act1 ("Recombinant") purified from *P. pastoris*, in the presence or absence of *S. cerevisiae* profilin (Pfy1) and formin (Bnr1). All reactions contained 10% Oregon green labelled skeletal muscle actin as a tracer. Data are averaged from 3 independent experiments (n = 10 filaments per experiment; 30 total). Error bars, SE. **(D)** Actin filament elongation rates calculated from reactions in (C).

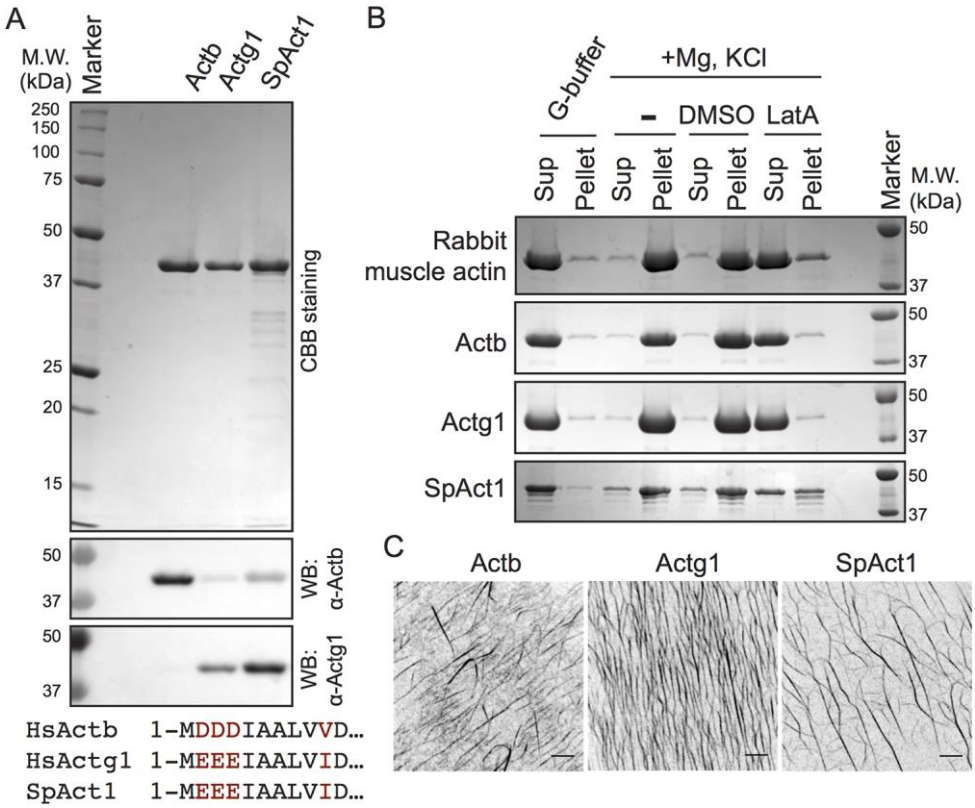

Figure 2. Purification of recombinant human non-muscle actins and fission yeast Act1.

(A) CBB gel image showing purified recombinant human β- ("Actb"), human γ ("Actg1") and *Schizosaccharomyces pombe* (SpAct1) actins. Immunoblotting in the bottom panels was performed with antibodies against Actb or Actg1 raised against peptides corresponding to the N-terminus of human β- and γ-actins. Since the N-terminus of *S. pombe* Act1 has strong similarity human γ-actin, the anti-Actg1 antibody could recognize *S. pombe* Act1 as well as γ-actin (see bottom alignment). **(B)** Actin sedimentation assays. Purified actin in low ionic strength buffer ("G-buffer") was mixed with KCl, EGTA and Mg^{2+} to induce actin polymerization. Actin sedimentation was tested in the presence of 0.5 mM Latrunculin A ("LatA"), solvent control ("DMSO") and in the absence of DMSO or Latrunculin A ("-"). After ultracentrifugation, actin in the pellet ("Pellet") and supernatant ("Sup") fractions were detected by CBB staining following SDS-PAGE. Rabbit muscle actin was used as a positive control. **(C)** Visualization of F-actin. The specified actins were incubated with KCl, EGTA and Mg^{2+} in the presence of 2% PEG and F-actin in all cases was stained with rhodamine-phalloidin and imaged using a Nikon inverted microscope fitted with a Yokogawa spinning disk head and an Andor iXon camera. Scale bar =5 µm.

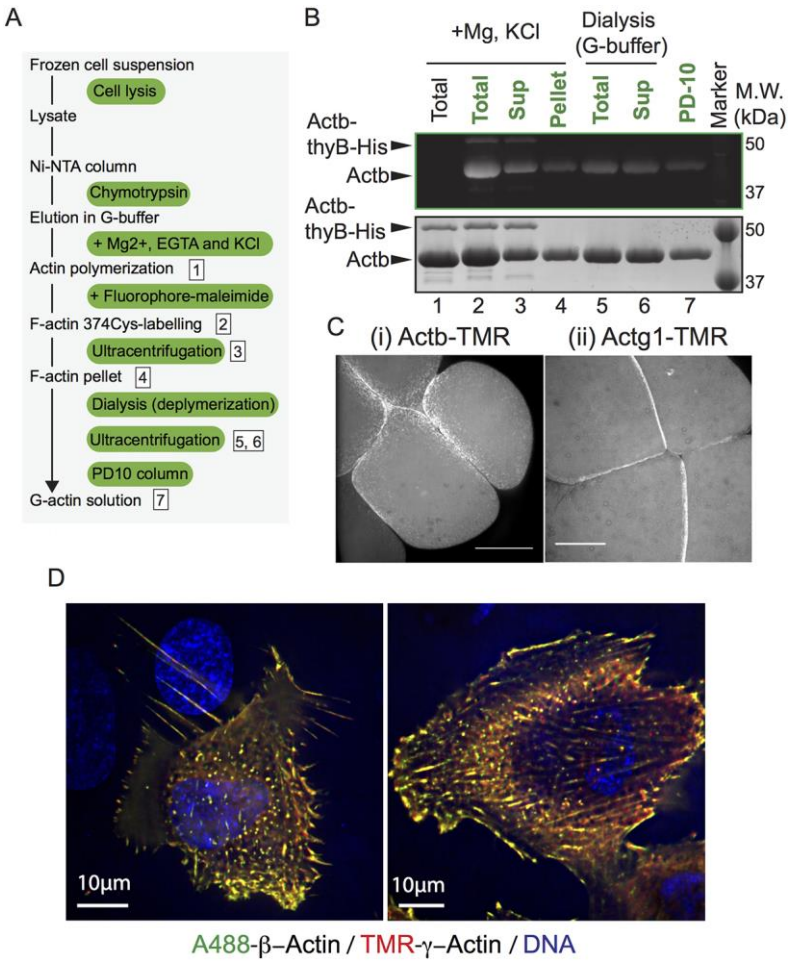

Figure 3. Recombinant actins were incorporated into actin cytoskeleton networks in cells.

(A and B) Schematic representation and gel image of actin Cys374 labelling method (details are shown in Materials and Methods). Eluates collected after chymotrypsin treatment (see Figure 1A) were mixed with KCl and Mg^{2+} to induce polymerization of β-actin (Lane 1) and incubated with Alexa Fluor 488 C5 maleimide to label the 374^{th} amino acid residue of β-actin in F-actin (Lane 2). The reaction mixture was spun in an ultracentrifuge to pellet down F-actin (Lane 3, supernatant ["Sup"]; Lane 4, pellet fraction ["Pellet"]). The pellet fraction was suspended in low salt buffer, G-buffer, and dialyzed against the same G-buffer. The dialyzed sample (Lane 5) was ultracentrifuged to remove F-actin (Lane 6). Free Alexa Fluor 488 C5 maleimide was removed by desalting column (Lane 7, "G-25"). **(C)** Microinjection of β-actin (i) and γ-actin (ii) labelled with TMR into zebrafish embryos. Images were acquired using a spinning disc confocal microscope. Scale bar =100 µm. **(D)** Injection of fluorescently labelled β- and γ-actins into RPE1 cells. β- and γ-actin were labelled with Alexa Fluor 488 and TMR, respectively and injected into human RPE1 cells. Left panel shows maximum projection of all z-axis stacks. Right panel shows maximum projection of 24 to 26^{th} z-axis stacks. Scale bar =10 µm.

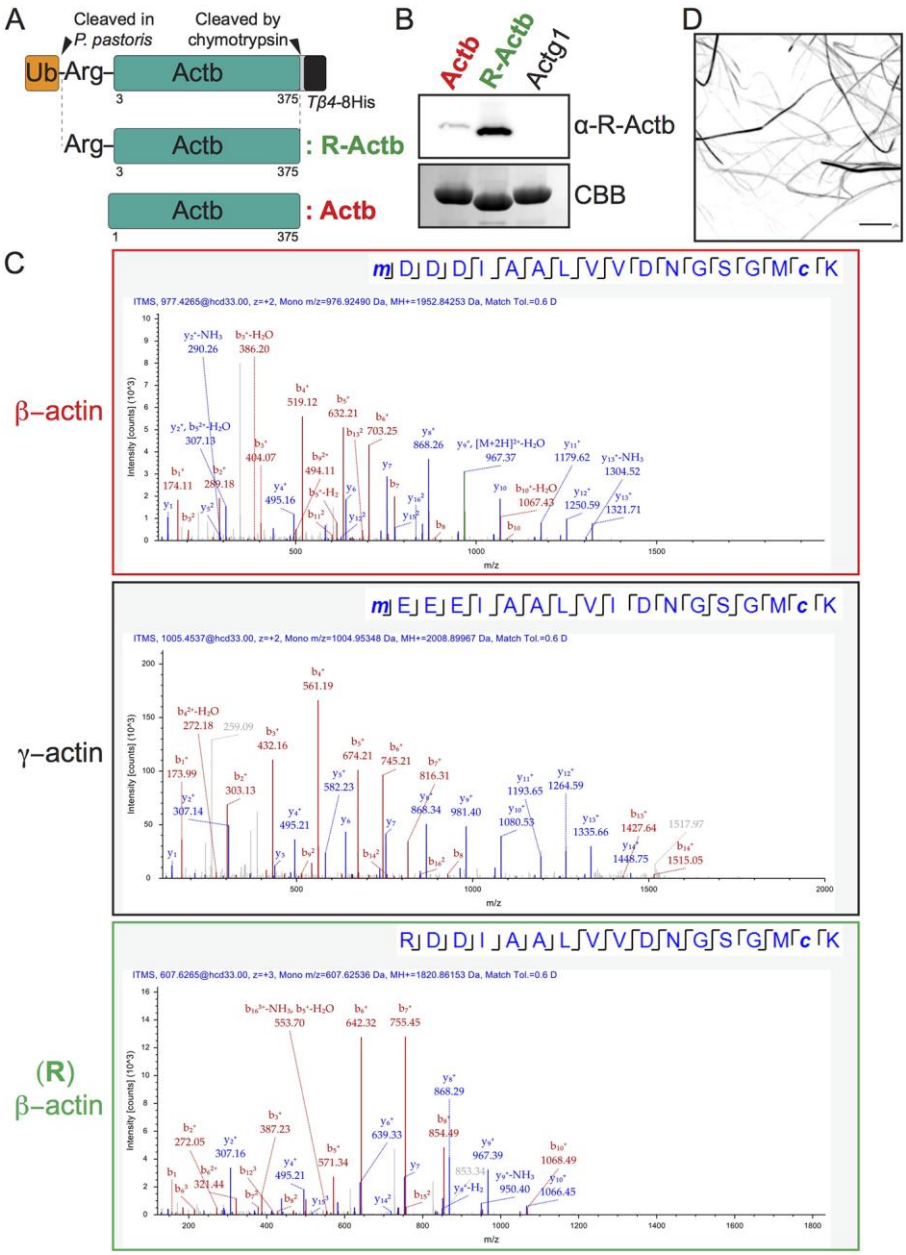

Figure 4. Purification of arginylated β-actin

(A) Schematic representation of expression of arginylated β-actin (R-Actb). **(B)** Immunoblotting and CBB staining showing purified R-Actb. Immunoblotting was performed with polyclonal antibodies against arginylated β-actin. **(C)** Representative mass spectra of the unique N-terminal tryptic peptide of β-actin, γ-actin and arginylated β-actin ("(R) β-actin") using HCD fragmentation. The N-terminal (R) β-actin tryptic unique peptide showed the substitution of Met-Asp by Arg. **(D)** Visualization of arginylated actin (R-Actb) filament. R-Actb were incubated with KCl, EGTA and Mg^{2+} in the presence of 2% PEG and stained with Cy5-phalloidin. Scale bar =5 μm.

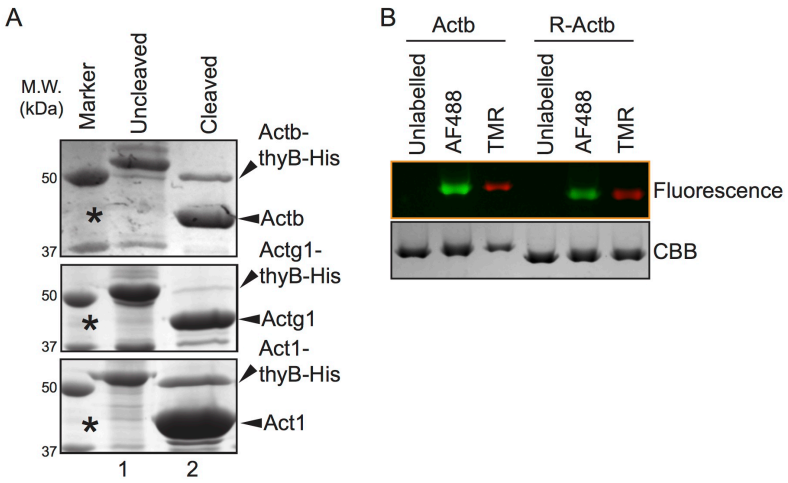

Supplemental figure 1. Purification of fission yeast Act1 and human non-muscle actins
(A) Endogenous P. pastoris actin does not co purify with the expressed recombinant actin. Proteins bound on nickel beads were eluted with SDS-PAGE sample buffer just before chymotrypsin cleavage and analysed by SDS-PAGE and CBB staining (Lane 1). Eluates collected after chymotrypsin treatments were also loaded on SDS-PAGE gel (Lane 2). Note that a 43 kDa protein is visualized only after cleavage with chymotrypsin and not in the uncleaved sample, establishing that P. pastoris actin does not co-purify detectably.
(B) Fluorescent labelling of arginylated beta-actin with Alexa Fluor 488 C5 maleimide and TMR-5-maleimide.

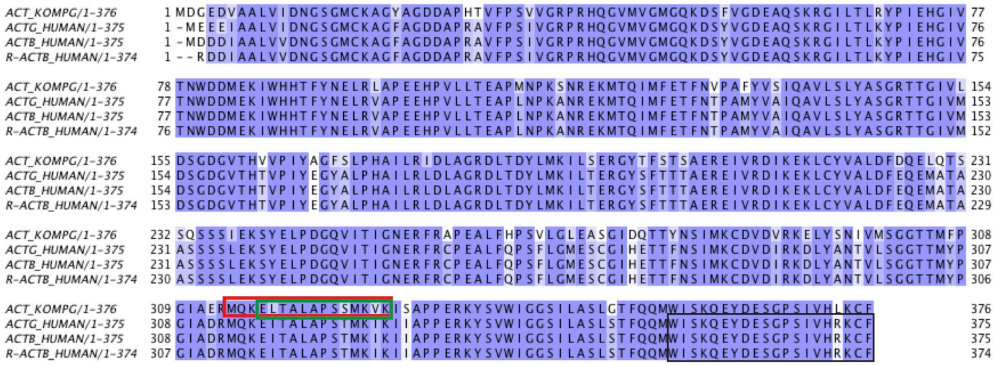

Supplemental figure 2. NanoLC-ESI-MS/MS analysis of actin proteins
Alignment of amino acid sequence of *P. pastoris* Act1 (ACT_KOMPG), β-actin (ACTB_HUMAN), γ-actin (ACTG_HUMAN), and arginylated β-actin (R_ACTB). Mass spectrometry identified tryptic peptides that covered the entire human β, γ, and R-β-actins. The only exception was the C-terminal CF residues, which were identified as part of a larger C-terminal peptide recovered upon cleavage the SDS-PAGE purified sample containing unfolded actin with chymotrypsin (black box).
The Pichia pastoris actin is predicted to contain ~ 6 unique peptides upon cleavage with trypsin that differentiate it from human β and γactins. We only found one area in all mass spectrometry experiments that may be consistent with arising from *P. pastoris* actin, marked with red and green boxes. In this area it was possible to assigned spectra to two miscleaved peptides with suggested methylation modifications (+14 Da). However, the same spectra could also be assigned to the human actins without additional methylation because there are two amino acid differences between human and *P. pastoris* sequences in this area, both with a molecular mass difference of 14 Da (serine to threonine and valine to isoleucine). It is possible that there may be a trace of *P. pastoris* methylated actin in the recombinant actin preparations. However, the simplest explanation, consistent with all observed spectra, is that un-methylated human actin (not *P. pastoris* actin) has been identified.

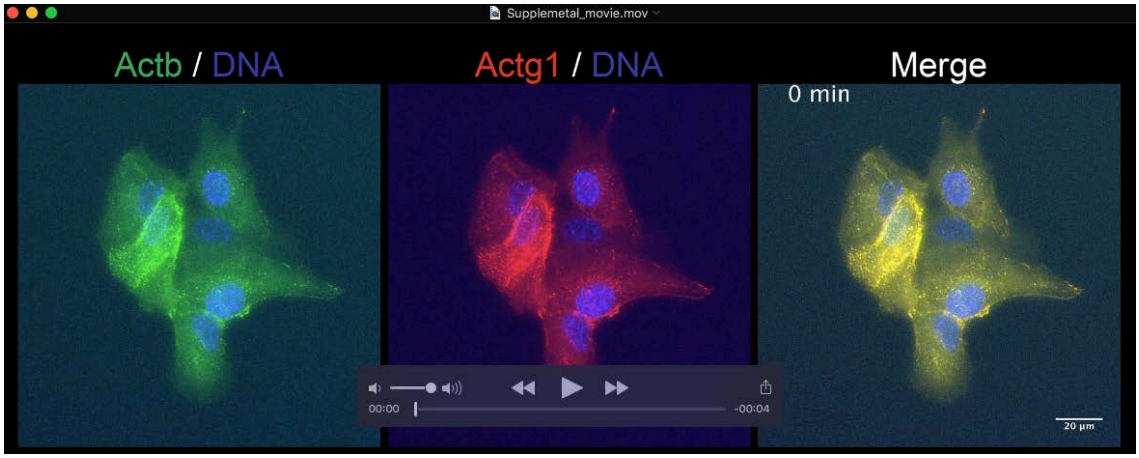

Supplemental movie. Time-lapse images of RPE cells injected with fluorescent labelled β- and γ-actins.

Time lapse images of microinjected β- and γ-actins in RPE cells. β- and γ-actin were labelled with Alexa Fluor 488 and TMR, respectively and injected into human RPE cells. Scale bar =20 µm. Images were acquired every 10 minutes.

Supplemental table 1. Peptides from trypsin-digested samples detected by mass spectrometric analysis.

Click here to Download Table S1

Supplemental table 2. Peptides from chymotrypsin-digested samples detected by mass spectrometric analysis.

Click here to Download Table S2